

# Higgs self coupling measurement in $e^+e^-$ collisions at center-of-mass energy of 500 GeV

C. Castanier<sup>(a)</sup>, P. Gay<sup>(a)</sup>, P. Lutz<sup>(b)</sup>, J. Orloff<sup>(a)</sup>

<sup>(a)</sup> *Laboratoire de Physique Corpusculaire, Univ. B. Pascal/IN<sup>2</sup>P<sup>3</sup>-CNRS,  
24 Av. des Landais, F-63177 Aubière Cedex, France*

<sup>(b)</sup> *CEA/DAPNIA, Service de Physique de particules,  
CE-Saclay, F-91191 Gif-sur-Yvette Cedex, France*

## Abstract

Feasibility of the measurement of the trilinear self-couplings of the Higgs boson is studied. Such a measurement would experimentally determine the structure of the Higgs potential. Full hadronic and semi-leptonic final states of the double-Higgs strahlung have been investigated.

# 1 Introduction

In the framework of the standard model, the generation of mass occurs through the Higgs mechanism. This mechanism assumes a Higgs potential,  $V(\Phi)$ , which behaves as  $V(\Phi)=\lambda(\Phi^2-\frac{1}{2}v^2)^2$ , where  $\phi$  is an isodoublet scalar field, and  $v\sim 246$  GeV is the vacuum expectation value of its neutral component. A determination of the Higgs boson mass, which satisfies  $m_h^2=4\lambda v^2$  at tree level in the standard model, will provide an indirect information about the Higgs potential and its self-coupling  $\lambda$ . The measurement of the trilinear self-coupling  $\lambda_{hhh}=\frac{6}{\sqrt{2}}\lambda v$  offers an independent determination of the Higgs potential shape. In case of disagreement, the comparison between these two measurements would give an interesting clue about new physics, like super-symmetry for instance. Anyway, the reconstruction of the Higgs potential is an essential step in the experimental validation of the Higgs mechanism that lies at the core of the standard model.

The aim of our study is to demonstrate how to measure the trilinear self-coupling  $\lambda_{hhh}$  in  $e^+e^-$  collisions at center-of-mass energies delivered by the future Linear Collider. The note is organized as follows : the framework of the study is defined in Section 2. The Monte Carlo simulation is reported in Section 3. Analyses and results are described in Section 4 and 5.

## 2 Signal

The trilinear Higgs self-coupling,  $\lambda_{hhh}$ , could be extracted from the measurement of the cross-section of each of the following processes : double Higgs-strahlung ( $e^+e^- \rightarrow Zhh$ ) or  $WW$  double-Higgs fusion ( $e^+e^- \rightarrow \bar{\nu}_e\nu_e hh$ ) [1]. Figure 1 indicates the major Feynman diagrams involved in the first process.

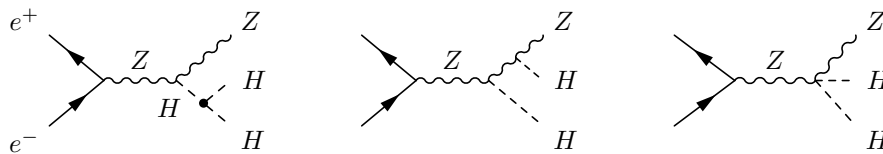


Figure 1: Feynman diagrams involved in the  $e^+e^- \rightarrow hhZ$  cross-section via the double Higgs-strahlung.

For light Higgs boson masses, the Higgs boson decays predominantly in a  $b\bar{b}$  pair. When the  $Z$  decays in a lepton pair, the final state is  $hhZ \rightarrow b\bar{b}b\bar{b}\ell^+\ell^-$ . With a high  $b$  content and two leptons, this topology produces an easy signature but represents only  $\sim 8\%$  of the total final state. By contrast, the  $hhZ \rightarrow b\bar{b}b\bar{b}q\bar{q}$  final state benefits from a high statistics with  $\sim 60\%$  of the final states but requires a more complicated analysis.

In the minimal super-symmetric extension (MSSM) of the standard model, the Higgs sector is richer with three neutral Higgs bosons ( $h$ ,  $H$  and  $A$ ). The Higgs potential is therefore more intricate and further trilinear self couplings are possible beyond  $\lambda_{hhh}$  :  $\lambda_{hhH}$ ,  $\lambda_{HHH}$ ,  $\lambda_{hAA}$ , and  $\lambda_{HAA}$ . At the tree level, these depend on two parameters ( $\tan\beta$  and  $m_A$  for instance). The radiative corrections are driven mainly by the top quark, so that the stop mass effectively

constitutes a third one. Studies performed in the parameter space of the MSSM are described in Ref. [1, 2]. Here, let us simply recall on Fig. 2 the sensitivity of  $\lambda_{hhh}$  as a function of  $m_A$  with different  $m_{\tilde{t}}$  assumptions. For fixed  $m_h$ , the value of  $\lambda_{hhh}$  reaches its standard model value for large  $m_A$  (decoupling limit), and the dependence on  $m_{\tilde{t}}$  only shows up for smaller values of  $m_A$ . However, the topologies obtained will be similar to the standard model ones, except for particular parameter choices where the Higgs boson decay into a  $b\bar{b}$  pair is suppressed. Thus, the experimental study we develop in this note, though a priori restricted to the standard model framework, is also relevant for the MSSM.

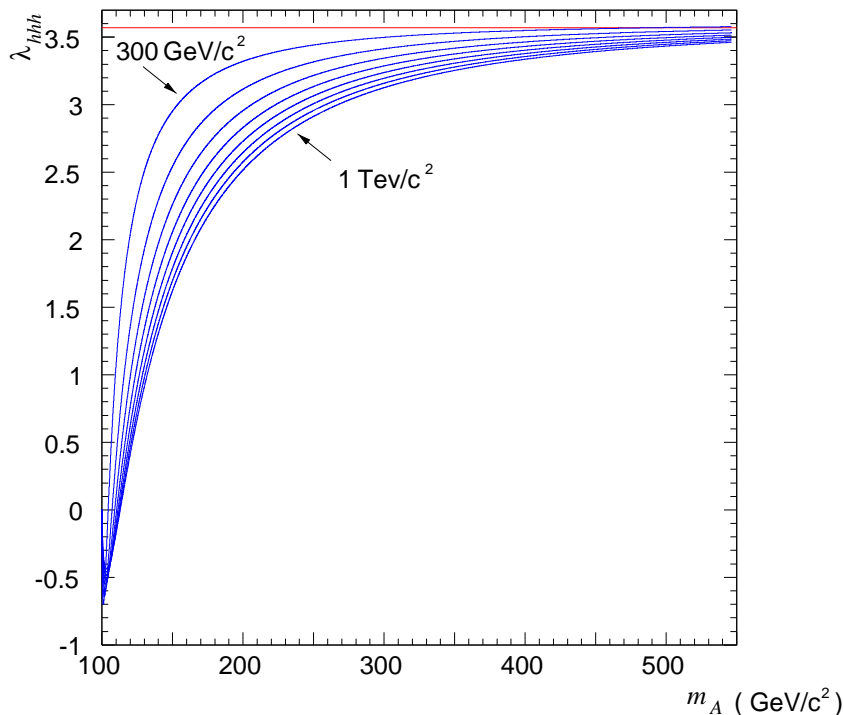


Figure 2: MSSM trilinear Higgs self-coupling ( $\lambda_{hhh}$ ) as a function of the mass of the pseudo-scalar Higgs boson mass ( $m_A$ ) and different assumptions of  $m_{\tilde{t}}$  from  $300 \text{ GeV}/c^2$  to  $1 \text{ TeV}/c^2$  with a  $100 \text{ GeV}/c^2$  step size; the horizontal line corresponds to the standard model value of  $\lambda_{hhh}$ . A  $100 \text{ GeV}/c^2$  Higgs boson mass has been assumed.

If the mass of the Higgs boson is assumed to be light ( $\sim 120 \text{ GeV}/c^2$ ) then the best center-of-mass energy is around  $500 \text{ GeV}$  [1] and the double Higgs-strahlung process cross-section is one order of magnitude greater than the WW fusion one. The study presented here will be performed for  $m_h=120 \text{ GeV}/c^2$  and  $\sqrt{s}=500 \text{ GeV}$  and it is restricted to the standard model framework.

Nevertheless, with  $m_h=120 \text{ GeV}/c^2$  and  $\sqrt{s}=500 \text{ GeV}$  the  $e^+e^- \rightarrow hhZ$  cross-section is still very tiny with a  $0.18 \text{ fb}$  value. Namely, for an expected integrated luminosity of  $500 \text{ fb}^{-1}$ , only 93 signal events are produced. The difficulty is increased by the the huge background sources, as detailed in next Section.

process	$N_{gen}$	$\sigma$ (fb)	generator	$\mathcal{L}_{sim}(\text{fb}^{-1})$
Signal				
hhZ ( $Z \rightarrow q\bar{q}$ )	11k	0.13	GRACE	$84.10^3$
hhZ ( $Z \rightarrow \ell^+\ell^-$ )	5k	0.02	GRACE	$270.10^3$
2 fermions				
$Z\gamma$	4.2M	8200.	PYTHIA	514.
$Z\gamma \rightarrow t\bar{t}\gamma$	150k	550.	PYTHIA	2145.
4 fermions				
WW	3.9M	7700.	PYTHIA	509.
WW $\rightarrow$ Wtb	17k	16.8	PYTHIA	$12.10^3$
ZZ	300k	550.	PYTHIA	545.
We $\nu$	2.6M	5300.	PYTHIA	502.
Zee	3.7M	7400.	PYTHIA	504.
hZ	35k	70.5	HZHA	1631.
$t\bar{t}h$ , hZ $\rightarrow$ $t\bar{t}h$	3k	0.4	GRACE	7500.
6 fermions				
WWZ ( $Z \rightarrow q\bar{q}$ )	21k	19.8	GRACE	3383.
WWZ ( $Z \rightarrow \ell^+\ell^-$ )	8.6k	2.8	GRACE	$10.10^3$ .
ZZZ ( $Z \rightarrow q\bar{q}$ )	6k	0.53	GRACE	$30.10^3$ .
ZZZ ( $Z \rightarrow \ell^+\ell^- \nu\bar{\nu}$ )	9.5k	1.01	GRACE	$28.10^3$ .

Table 1: Cross-sections for signal and background processes, Monte Carlo statistics and simulated luminosity ( $\mathcal{L}_{sim}$ ).

### 3 Simulation

The signal event samples have been simulated with the **GRACE** generator [4]. The background sources are either two fermions final state processes as  $e^+e^- \rightarrow Z\gamma$ , or four fermions processes like  $e^+e^- \rightarrow W^+W^-$ , ZZ, We $\nu$ , Zee, hZ. The latter has been simulated with **HZHA** generator [5] while **PYTHIA** [6] was used for the others processes. Six fermions final state processes like  $e^+e^- \rightarrow WWZ$  or ZZZ are also background sources and **GRACE** was used to simulate them. Table 1 summaries the size of the samples used and the cross-section of each process. Since  $e^+e^- \rightarrow t\bar{t}$  and  $e^+e^- \rightarrow Wtb$  will yield major contributions to the background, an emphasis has been performed and a simulated luminosity greater than  $2000\text{fb}^{-1}$  was generated for such processes as well as for six fermions processes while for the others a simulated luminosity greater than  $500\text{fb}^{-1}$  was used as reported in Table 1. Even if the cross-section is small,  $e^+e^- \rightarrow t\bar{t}h$  process is also a potential source of background and this process was considered.

The detector simulation was performed with a Parametric Monte Carlo [7]. The tracking system, immersed in a 3 tesla magnetic field, consists on a vertex detector (VDET) surrounding the beam tube at  $\sim$  one centimeter radius followed by a time projection chamber (TPC). The VDET impact parameter resolution is assumed to be  $\sim 5\mu\text{m}$  in both rz and r $\phi$  views. Only charged particles with a transverse momentum greater than 0.2 GeV/c are reconstructed. The tracking efficiency is assumed to be 99.7%. The tracking system is complemented with a forward

tracker and muon chambers. The b-tagging is performed through a parametrisation derived from full reconstruction [8].

At low angle, a luminometer (LCAL) enforces the hermeticity of the detector. Energy and direction of the photons and neutral hadrons are measured thanks to the electromagnetic (ECAL) and hadronic (HCAL) calorimeters. The intrinsic energy resolutions taken into account are  $\Delta E/E=10.2\%/\sqrt{E(GeV)}$  and  $\Delta E/E=40.5\%/\sqrt{E(GeV)}$  respectively for ECAL/LCAL and HCAL. The energy threshold below which no neutral particles is reconstructed in calorimeters are 200 MeV and 500 MeV for ECAL and HCAL respectively. Following studies performed with full simulation of high granularity calorimeters [9], a jet energy resolution of  $40\%/\sqrt{E_{jet}}$  could be achieved. Such a resolution has been assumed in the analysis described hereafter.

## 4 Analyses

If an isolated track is allowed to form a jet, both final state,  $hhq\bar{q}$  and  $hh\ell^+\ell^-$  are characterized by six jets, and the hadronic system is characterized by a high b content.

The analysis works in three steps. The preselection mainly based on event shape variables consists in removing most of the two- and four-fermions final-state contributions of the background. In a second step the b-content as well as the di-jets reconstructed masses are used to reject the three-bosons final-state contribution. Finally, all the relevant informations are combined with a multivariable method.

The preselection consists in rejecting events with a charged multiplicity less than 30. The thrust value has to be less than 0.9 and the direction of the thrust with respect to beam axis should verify  $\cos(\theta_{thrust}) < 0.9$ . In order to remove  $e^+e^- \rightarrow Z(\gamma)$ , the longitudinal component of the total momentum of the event ( $P_z^{tot}$ ) have to satisfy  $P_z^{tot} < 50$  GeV/c. The event is divided in two hemispheres with respect to the thrust axis and the invariant mass of each hemisphere ( $M_{hemi}$ ) must exceed 90 GeV/c<sup>2</sup>. Figure 3 illustrates the discrimination between the signal and the background processes achieved by this variable.

The event is clustered with the DURHAM scheme. The variation of the  $y_{cut}$  is stopped when the transition between six and seven jets occurs and the event is thus forced into a six jets topology. To eliminate  $e^+e^- \rightarrow Z(\gamma)$  with a photon emitted in the sensitive region of the ECAL, a fraction of electromagnetic energy with respect to the jet energy less than 80% is requested for all the jets.

The numbers of events expected from background processes at the preselection level are reported in Table 2. The contribution from  $e^+e^- \rightarrow Zee$  or  $We\nu$  processes is canceled. Around  $48.10^3$  background events are expected with a luminosity of  $500 \text{ fb}^{-1}$  while  $\sim 42$  and  $\sim 7$  signal events are expected for  $hhq\bar{q}$  and  $hh\ell^+\ell^-$  final state respectively when  $m_h=120\text{GeV}/c^2$  is assumed. Major sources of background are processes with at least one top quark in the final state. In fact, 99% of the contribution from the  $e^+e^- \rightarrow Z(\gamma)$  process is coming from  $Z \rightarrow t\bar{t}$  and 80% of the contribution from  $e^+e^- \rightarrow W^+W^-$  process is  $e^+e^- \rightarrow Wtb$ . The remaining part of those background processes mainly consists in six fermions final state with two or one b quarks. However, even if the background contribution is largely reduced, the remaining part is three order of magnitude greater than the signal.

Thanks to the jet energy flow resolution, a direct use of the reconstructed di-jets masses is applied. Among all the di-jets masses in the event, the so-called  $m_{56}$  mass minimizes the

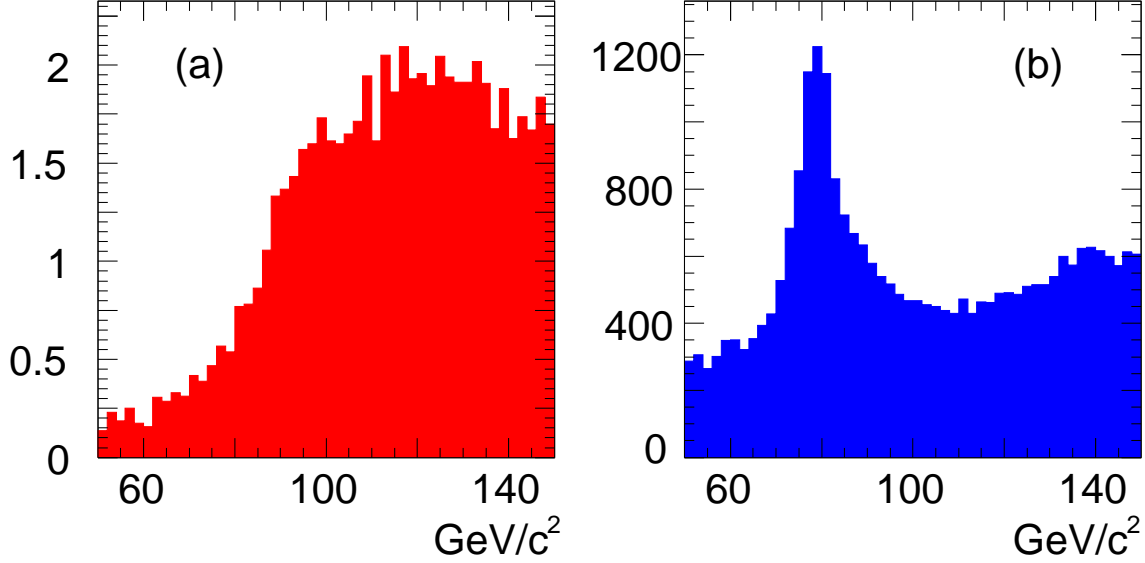


Figure 3: Distribution of the invariant mass of each hemisphere ( $M_{\text{hemi}}$ ) for (a) signal and (b) background processes.

difference with a  $m_Z$  hypothesis. The b content of the system recoiling to the Z ( $\mathcal{B}^{\text{recoil}}$ ) is an excellent variable to reject contribution from background processes. In a first stage, a loose cut is applied : at least one b jet among the recoiling jets system ( $\mathcal{B}^{\text{recoil}} > 1$ ) is requested. Among the four jets recoiling to the Z (*i.e.*  $m_{56}$ ), the di-jets masses  $m_{12}$  and  $m_{34}$  are defined by minimizing  $\|m_{12} - m_{34}\|$  while having both  $m_{12}$  and  $m_{34}$  larger than 100  $\text{GeV}/c^2$ . The three di-jets masses are combined in a simple way in order to form the distance  $\text{DIST} = \sqrt{((m_{12} - m_h)^2 + (m_{34} - m_h)^2 + (m_{56} - m_Z)^2)}$ , where  $m_h$  and  $m_Z$  are the Higgs boson and Z masses. The distribution of this variable DIST is displayed on Fig. 4 when a tightened cut on  $\mathcal{B}^{\text{recoil}}$  is applied ( $\mathcal{B}^{\text{recoil}} > 2$ ).

The contribution from the various background sources are reported in Table 2 for the loose ( $\mathcal{B}^{\text{recoil}} > 1$ ) and tightened ( $\mathcal{B}^{\text{recoil}} > 2$ ) cuts. The signal efficiencies are 43% and 35% respectively. Most of the background is coming from  $e^+e^- \rightarrow Wtb$  and  $e^+e^- \rightarrow t\bar{t}$  processes while the six fermions final state contribution is due to  $e^+e^- \rightarrow ZZZ$  with relatively small level with respect to the previous contributions. The figure of merit defined as  $s/\sqrt{b}$  increases from 0.22 at the preselection level up to 3, with an integrated luminosity of 500  $\text{fb}^{-1}$ .

Clearly the combination of the the di-jets masses in the DIST variable is a very crude one. Thus, in order to take into account the correlation between the di-jets masses and the b content of the event, the variables  $m_{12}$ ,  $m_{34}$ ,  $m_{56}$  and  $\mathcal{B}^{\text{recoil}}$  are combined with a multivariable method. Here a neural network (NNet) approach has been adopted. The NNet output varies from -1 (background-like) to +1 (signal-like). Restricted to the positive values, Fig. 5 displays the NNet output from signal and background processes while the contributions from the background sources are indicated in Table 2. The signal efficiency is about 36% and  $s/\sqrt{b}$  is  $\sim 4.2$  when an integrated luminosity of 500  $\text{fb}^{-1}$  is assumed. The clear discrimination between the signal and the background processes could be exploited to reinforce the figure of merit : as an example, with the same integrated luminosity, a cut on the NNet output at 0.5 leads to 31 signal events while 27 background events are expected corresponding to a figure of merit of  $\sim 6$ . Better

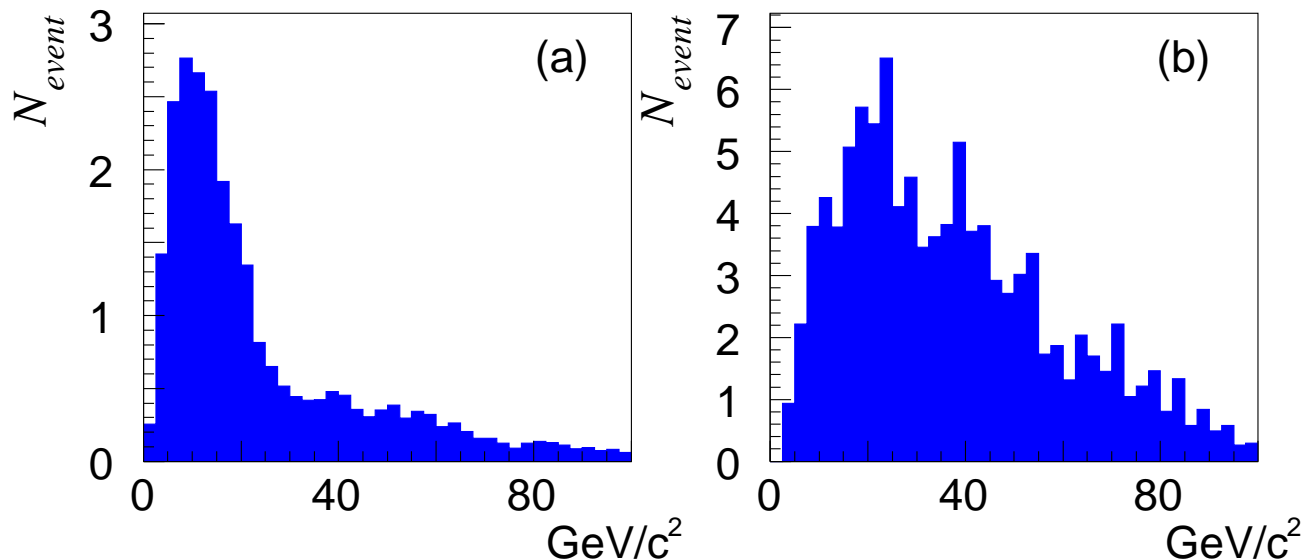


Figure 4: *Distribution of the variable DIST (defined in text) for (a) signal and (b) background processes.*

values could be obtained with tightened cuts and this behavior is fully used in the cross-section measurement where a fit of the NNet output distribution is performed as indicated in the next Section.

## 5 Results

The cross-section of the  $e^+e^- \rightarrow hhZ$  have to be measured, in order to extract  $\lambda_{hhh}$ . Such a measurement is performed by a likelihood fit of the characteristic variable (DIST,  $\mathcal{B}^{\text{recoil}}$ ,  $\text{NN}_{\text{output}}$ ) already used in the analysis. The different selections (indexed as B, C and D in Table 2) have been tested. The relative error obtained on the cross-section measurement ( $\Delta\sigma/\sigma$ ) according to the different sets of 'selection/discriminant variable' are reported in Table 3 for integrated luminosity from 500 to 2000  $\text{fb}^{-1}$ . A relative error of 10.3% on the cross-section is obtained when NNet selection is used and an integrated luminosity of 2  $\text{ab}^{-1}$ .

With the same analysis used for  $m_h=120 \text{ GeV}/c^2$ , the relative error on the  $e^+e^- \rightarrow hhZ$  cross-section has been evaluated for higher Higgs boson masses up to 140  $\text{GeV}/c^2$ . The relative errors are reported in Table 4 as well as the cross-section values and expected number of events with an integrated luminosity of 500  $\text{fb}^{-1}$ . Only the 'B/ $\mathcal{B}^{\text{recoil}}$ ' set of selection/variable has been considered. Due to the decrease of the cross-section the error increases rapidly up to 17% even with an integrated luminosity of 2  $\text{ab}^{-1}$ . Since this result is obtained with a standard selection, a dedicated analysis based on retrained NNet which take into account the Higgs boson mass would improve the performances.

To derive the relative error on  $\lambda_{hhh}$  ( $\Delta\lambda/\lambda$ ) the relation between  $\lambda_{hhh}$  and the cross-section has to be taken into account according the behavior displayed on Fig. 6 [10] where  $\kappa$  is  $\lambda_{hhh}$  expressed in unit of  $\lambda_0$ , the trilinear Higgs coupling in the standard model. Thus, on this Fig. 6,  $\kappa=1$  stands for the standard model. Furthermore, the incoming beams on that figure

process	preselection	b-content $\mathcal{B}^{\text{recoil}} > 1$	b-content $\mathcal{B}^{\text{recoil}} > 2$	NNet >0
hhq $\bar{q}$	41.4	34.	27.1	27.5
hh $\ell^+\ell^-$	6.7	6.2	5.1	6.4
total hhZ	49.1	40.2	32.2	33.9
WW	2114.	233.	74.3	32.
Z $\gamma$	44938.	116.	34.	24.
ZZ	484.	7.4	0.	0.
WWZ	331.	0.6	0.	0.14
ZZZ	56.6	19.	9.	8.4
hZ	174.	0.	0.	0.
t $\bar{t}$ h	3.	0.	0.	0.
total bkg.	48089.	376.	117.4	64.3
s/b	0.1%	11%	27%	53%
s/ $\sqrt{b}$	0.22	2.	3.	4.2
selection index		B	C	D

Table 2: Numbers of events with  $\mathcal{L} = 500\text{fb}^{-1}$  expected both for signal and background processes at preselection level, standard selections (two set of cut on  $\mathcal{B}^{\text{recoil}}$ ) and multivariable analysis; s/b and s/ $\sqrt{b}$  are also indicated.

selection	variable	$\Delta\sigma/\sigma$		
		$\mathcal{L} = 500\text{fb}^{-1}$	$1000\text{fb}^{-1}$	$2000\text{fb}^{-1}$
B	DIST	32.8 %	25.6 %	17.7 %
C	DIST	29.8 %	21.5 %	15.1 %
B	$\mathcal{B}^{\text{recoil}}$	24.1 %	17.3 %	11.6 %
D	NN output	20.4 %	12.9 %	10.3 %

Table 3: Relative error ( $\Delta\sigma/\sigma$ ) on  $\sigma_{hhZ}$  for different selection/variable set and integrated luminosities

are assumed to be fully polarized so that the displayed cross-section must be reduced by a factor two [1] to be coherent with the present unpolarized study.

As indicated by the Fig. 1, only one diagram for the  $e^+e^- \rightarrow hhZ$  cross-section is sensitive to  $\lambda_{hhh}$ . The others constitute an irreducible background for the  $\lambda_{hhh}$  measurement which shows up on Fig. 6 as the non-vanishing cross-section at  $\kappa = 0$ . Such an irreducible background makes the measurement intrinsically difficult.

From Fig. 6 the relative variations of the cross-section and  $\lambda_{hhh}$  around the standard model are related by  $\Delta\lambda/\lambda \sim 1.75 \times \Delta\sigma/\sigma$ . The relative error on  $\lambda_{hhh}$  is accordingly reported in Table 5 for two sets of selection/variable. With an integrated luminosity of  $2\text{ab}^{-1}$  and NNet output, the relative precision  $\Delta\lambda/\lambda$  is 18%, and relaxes to 22% with half of that luminosity.



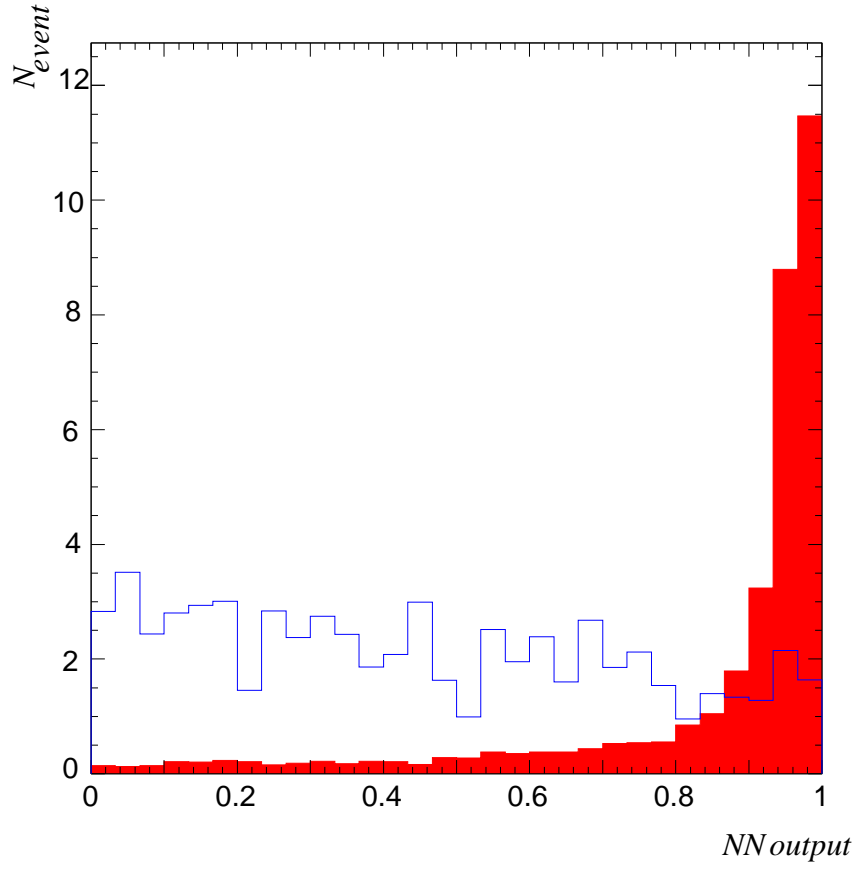


Figure 5: Neural Network output distribution ( $NN_{output}$ ) for HHZ signal (full histogram) and background (empty histogram) with  $500 \text{ fb}^{-1}$  and  $m_h=120 \text{ GeV}/c^2$ .

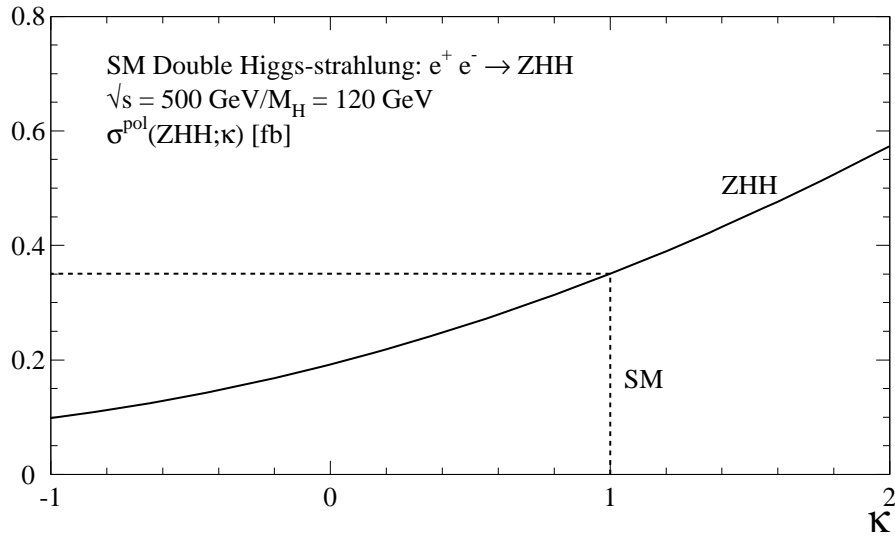


Figure 6:  $e^+e^- \rightarrow hhZ$  cross-section (in fb) as a function of  $\kappa$  when the incoming beams are fully polarized;  $m_h=120 \text{ GeV}/c^2$  and  $\sqrt{s}=500 \text{ GeV}$ .

$m_h(\text{GeV}/c^2)$	$\sigma_{hhZ}(\text{fb})$	$N_{hhZ}^{500}$	$\epsilon_{hhZ}$	$\Delta\sigma/\sigma$		
				$\mathcal{L}=500\text{fb}^{-1}$	$1000\text{fb}^{-1}$	$2000\text{fb}^{-1}$
120	0.186	93.	43%	24.1%	17.3%	11.6%
130	0.149	74.	43%	26.6%	19%	17.7%
140	0.115	57.	39%	32%	23%	17%

Table 4: Relative error ( $\Delta\sigma/\sigma$ ) on  $\sigma_{hhZ}$  with the ' $\mathcal{B}/\mathcal{B}^{\text{recoil}}$ ' set for different Higgs boson masses and integrated luminosities; signal efficiencies ( $\epsilon_{hhZ}$ ) and cross-sections ( $\sigma_{hhZ}$ ) are reported and ( $N_{hhZ}^{500}$ ) the expected number of hhZ events with  $\mathcal{L}=500\text{fb}^{-1}$

selection	variable	$\Delta\lambda/\lambda$		
		$\mathcal{L}=500\text{fb}^{-1}$	$1000\text{fb}^{-1}$	$2000\text{fb}^{-1}$
B	$\mathcal{B}^{\text{recoil}}$	42.2%	30.3%	20.3%
D	NN output	35.7%	22.6%	18.0%

Table 5: Relative error ( $\Delta\lambda/\lambda$ ) on  $\lambda_{hhh}$  for different selections and integrated luminosities.

## 6 Conclusions

To establish the Higgs mechanism in an unambiguous way, the self-energy potential of the Higgs field must be reconstructed. This implies the determination of the trilinear self-coupling. The experimental feasibility of the  $\lambda_{hhh}$  measurement has been explored through a detailed analysis of the reconstruction of the double Higgs-strahlung events. It takes advantage of the characteristic signature with four b jets and a Z boson, reconstructed either in its leptonic or hadronic decay modes. The large four and six fermion background and the tiny signal cross section make of this analysis a genuine experimental challenge. An excellent tagging as well as reconstruction capabilities of the TESLA detector are then essential. Thanks to a multivariable method, based here on a neural network (NNet), a  $s/\sqrt{b}=6$  could be achieved with 68 signal events selected in  $1000\text{fb}^{-1}$  with a center-of-mass energy of 500 GeV and  $m_h=120\text{GeV}/c^2$ ; 18% of the selected signal events are from  $hh\ell^+\ell^-$ . With help of high integrated luminosity ( $2\text{ab}^{-1}$ ), the determination of the  $e^+e^-\rightarrow hhZ$  cross-section with a 10% relative error could be achieved leading to a relative error on  $\lambda_{hhh}$  of 18%.

## Acknowledgements

We gratefully acknowledge discussions with M. Battaglia, A. Djouadi, M. Muhlleitner and P. Zerwas.

## References

- [1] A. Djouadi, W. Killian, M. Muhlleitner and P. Zerwas, Eur. Phys. J. C10
- [2] P. Osland, P.N. Pandita, Phys. Rev. D
- [3] D.J. Miller and S. Moretti RAL-TR-99-032, May 1999
- [4] GRACE manual, MINAMI-TATEYA group, KEK report 92-19, (1993)
- [5] P. Janot, The HZHA generator , in 'Physics at LEP', Eds. G. Altarelli, T. Sjöstrand and F. Zwinger, CERN 96-01 (1996) Vol.2, p.309
- [6] T. Sjöstrand, High-energy-physics event generation with PYTHIA 5.7 and JETSET 7.4, Compt. Phys. Commun.82 (1994) 74
- [7] M. Pohl, H.J. Schreiber, SIMDET.3 A Parametric Monte Carlo for a TESLA Detector, DESY 99-030 (1999)
- [8] R. Hawkings, Vertex detector and flavour tagging studies for the TESLA linear collider, LC-PHSM/2000-026
- [9] P. Gay, *Eflow with high granularity calorimeters*, talk given at Linear Collider Workshop 2000, Fermi National Accelerator Laboratory, October 24-28, 2000, Batavia, Illinois, USA; J-C. brient *et. al* , Si-W calorimeter performances, LC-Note/2000 *in preparation*
- [10] M. Muhlleitner, private communication